This is a pee-reviewed, author's accepted manuscript of the following research article:
Shao, Z., Ye, Z., Lu, H., & Fan, F. (2022).
Improved mechanical property and corrosion and wear resistance of high-voltage aluminium wires by micro-arc oxidation coating.
IEEE Transactions on Power Delivery, 1-11. https://doi.org/10.1109/TPWRD.2022.3213759

Improved Mechanical Property and Corrosion and Wear Resistance of High-Voltage Aluminium Wires by Micro-Arc Oxidation Coating

Zhonglei Shao, Zishuo Ye, Hailin Lu, and Fulin Fan

Abstract—**New surface treatments are required to improve the resistance of high-voltage aluminium conductors to corrosion and wear. This paper describes the preparation of ceramic coatings on the surface of aluminium wires by the micro-arc oxidation (MAO) technology. The surface morphology, mechanical and tribological properties, electrical resistivity, wear and corrosion resistance of the MAO-treated aluminium samples are examined and compared not only with the untreated samples but also between the use of different current densities in the MAO process. The MAO treatment can increase the tensile strength of the wire and mitigate the wire elongation at excessive high temperature. In addition, the increased surface hardness and the overlapping micro-porous distribution of the MAO coating improve the resistance of the treated sample to wear and corrosion respectively, protecting the aluminium substrate from the joint effects of wear and corrosion. Furthermore, the MAO coating has little impact on the electrical resistivity of aluminium conductors and can mitigate the resistivity change due to corrosive damage. The MAO technology providing a potential idea for the surface treatment of aluminium conductors is expected to extend the service life and alleviate maintenance needs of aluminium conductors operating in harsh environments.**

Index Terms—**Corrosion resistance, high-voltage aluminium conductors, mechanical properties, micro-arc oxidation coating, wear resistance.**

I. Introduction

THE deterioration of metal structures due to atmospheric corrosion is one of the most serious problems in the world today, causing hundreds of billions of dollars in damage every year [1], [2]. With high-voltage (HV) overhead lines (OHLs) facing an increasingly complex and deteriorating service environment, corrosion and wear damages are two of the main areas of OHL failures [3]. Aluminium and its alloys not only have the advantage of light weight, but also have good conductivity and excellent corrosion resistance, making them one of the most commonly used overhead conductor materials [4], [5]. However, due to the poor mechanical properties and wear resistance of aluminium and its lack of stability at high temperatures, surfaces made of the aluminium oxide are more prone to damage, eventually resulting in corrosion protection failures [6]-[8]. When the relative humidity of the atmosphere reaches a certain level, the moisture on the wire surface will slowly coalesce into a water film [9]. In a polluted environment, O_2, CO_2 and a small amount of H_2S, NH_2, SO_2, NO_2, Cl_2, HCl and other gases and salts in the atmosphere are dissolved in the water film, which transforms the wire surface from a water film into an electrolyte film [10], [11]. This reacts with the metal oxide film on the original layer of the wire, forming localised, small holes deep inside the metal and creating pitting corrosion [12]. Once a pitting hole is formed, the dissolution rate in the hole can rise to a dangerous level, often causing accidents and greater damages.

An easy-to-operate and cost-effective line surface protection technology is urgently required to improve the OHL corrosion resistance [13]. Coating the corrosion-prone conductor surface with materials that have good corrosion resistance is considered an effective approach. Materials such as fluorocarbon resins, silicone resins and epoxy resins can all be used as anti-corrosion coatings [14]-[16]. Although this approach is effective in preventing the corrosive medium from infiltrating the stranded wire, the weight of the wire may increase with the addition of anti-corrosion grease. In addition, the anti-corrosion coatings generally have poor adhesion to the substrate and will peel off with prolonged use. Traditional anti-corrosion coatings contain a lot of toxic substances, posing a huge threat to human health and ecological environments [17]. The techniques of sacrificial metal coating and zinc arc spraying are widely used in the field of corrosion protection by forming a dense adherent film (barrier protection) on the surface of a certain substrate, and are also applied to aluminium conductor steel reinforced (ACSR) conductors [18]. However, this treatment may worsen the durability and life cycle of ACSR conductors when they are placed in harsher environments such as industrial polluted areas and coastal areas. At the same time, contact corrosion will occur between the galvanized steel core and the contact layer of the aluminium strands due to the difference in the potential between metal electrodes [19]. Corrosion damages can produce white powder and pockmarks on the aluminium strands and their contact layers with the steel core, significantly reducing the mechanical properties of wires. This will not only cause major hazards such as broken strands and wires, but also reduces the service life of OHLs and increases the cost of metal plating [20].

Micro-arc oxidation (MAO), also referred to as plasma electrolytic oxidation (PEO), is an emerging surface treatment

(Corresponding authors: F. Fan and Z. Ye).
Z. Shao and F. Fan are with the Department of Electronic and Electrical Engineering, University of Strathclyde, Glasgow, G1 1XW, United Kingdom (e-mail: szl98981@gmail.com; f.fan@strath.ac.uk).
Z. Ye and H. Lu are with the Group of Mechanical and Biomedical Engineering, College of Mechanical and Electronic Engineering, Xi'an Polytechnic University, Xi'an, Shaanxi, 710048, P.R. China (e-mail: 15809255793@163.com; lu@xpu.edu.cn).

technology developed from anodic oxidation by immersing valve metals such as aluminium, magnesium and titanium in an electrolyte and using electrical energy to create spark discharge phenomenon in the discharge channel on the surface of the base metal film. Then a layer of insulating ceramic film resistant to wear, heat and corrosion is formed [21]-[24]. The aluminium and its alloys processed with the MAO technology have been examined in salt spraying tests and predicted to have a longer anti-corrosion lifetime than those treated by other approaches including anodic oxidation. By applying the MAO to the LY2 aluminium alloy, Wu et al. obtained a 20-μm dense aluminium oxide coating on the surface with small roughness (0.5 μm) and high Vickers hardness (1200 HV); the treated aluminium alloy having excellent corrosion resistance was observed to have a lifetime of up to 1800 hours and a passivation potential of more than 10 V in salt spraying tests, which were only 400 hours and 2 V respectively for the untreated wire [25]. Li et al. greatly improved the wear resistance of the 2024 aluminium alloy by employing different cathodic pulse widths in the MAO process, finding that the wear of the coating largely decreased with the cathodic pulse width [26].

In summary, the MAO technology can be applied to improve the corrosion and wear resistance of aluminium conductors by growing a ceramic layer in situ on the surface. Given a strong bond between the substrate and the film layer, the ceramic layer is not easy to peel off. Furthermore, the insulating ceramic layer isolates the outer part of aluminium wires in the ACSR from the steel core, avoiding the galvanic corrosion due to direct contact of dissimilar metals. However, detailed studies on mechanical and tribological properties of the MAO-coated aluminium wires are lacking in the existing literature. This paper performs an in-depth investigation into the surface microstructure, mechanical properties, electrical resistivity, wear and corrosion resistance of the aluminium wires with coating being prepared by different current densities in the MAO process [27], [28]. The alkaline solutions having a high film growth rate and low environmental pollution are used here as electrolytes in the MAO process [29], [30]. In addition, the potential annual cost saving of a particular ACSR OHL section with the MAO treatment are evaluated to reflect the economic benefits of an extended service life and reduced maintenance requirements. The MAO-based ceramic layer having excellent corrosion and wear resistance is of great market value for HV OHLs.

II. Experimental Details

A. Materials

Pure aluminium wires produced by Huaxing Metal Profiles Co., China with greater than 99.5wt% aluminium content were used as experimental materials. The electrolytes comprising sodium silicate, sodium hydroxide, sodium tungstate, ammonium metavanadate and polyethylene glycol (i.e., PEG, with an average molecular weight of 4000 Da) were provided by Tianjin Damao Chemical Reagent Factory, Tianjin, China. Distilled water was produced in the laboratory. All the materials and reagents used in the experiment were of analytical grade.

B. Sample Preparation

Prior to the MAO treatment, the aluminium wire sample with a length of 500 mm and a diameter of 1.5 mm was degreased by ultrasound in acetone, then cleaned by deionised water, and finally dried in an oven. Then the MAO process was performed by using a bipolar MAO power supply model FL7-MAOB60A (Jun Cheng Precision, China) with the aluminium wire and the electrolytic tank as anode and cathode respectively, as shown in Fig. 1. The current density and frequency were 0.4 A/dm^2 and 600 Hz respectively, with equal positive and negative duty cycles of 20%. The alkaline electrolyte consisted of 18 g/L sodium silicate, 4 g/L sodium hydroxide, 2 g/L sodium tungstate, 4 g/L ammonium metavanadate, and 1 g/L PEG. The MAO process was operated based on a constant voltage (CV)-constant current (CC) mode. Specifically, the MAO process started from the CV mode with an initial voltage of 100 V, which was then increased to 200 V and 300 V subsequently after the current stabilised until the arc initiation voltage was reached, as shown in Fig. 2(a); then the generation of the MAO coating increased the resistivity and when the current dropped to 3 A/dm^2, the CC mode was activated to keep the current at 0.4 A/dm^2 (see Fig. 2(b)), ensuring a continuous MAO process at a low current level which can avoid the adverse effects of long-term high currents on MAO coatings. Despite the current density drop at the start of the CC mode, the voltage across the aluminium wire kept increasing (see Fig. 2(a)) and sustaining the MAO process for the constant generation of MAO coatings. To examine the influence of the current density selected in the CC mode, the MAO process was additionally performed with a constant current of 0.8 A/dm^2, 1.2 A/dm^2, 1.6 A/dm^2, 2 A/dm^2 or 2.4 A/dm^2 respectively while other experimental parameters remained the same. In addition, a circulation cooling system worked continuously during the 10-min MAO treatment to avoid excess electrolyte temperature. Finally, the MAO-treated samples were cleaned with deionised water and dried in an oven. Three aluminium samples were processed at each current density so as to ensure the experiment reproducibility.

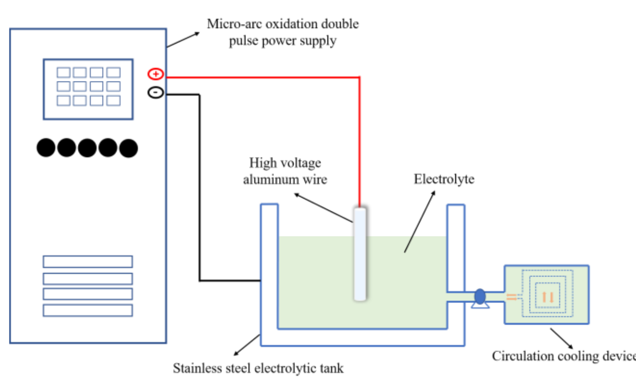

Fig. 1. The operating schematic of the MAO equipment set.

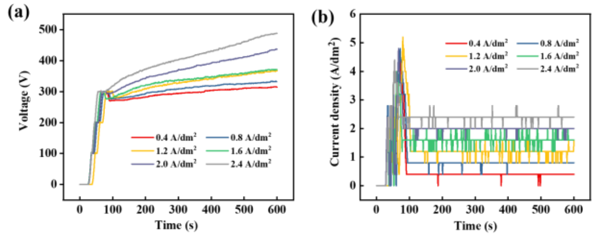

Fig. 2. Measurements of (a) transient voltage and (b) current density versus time given different current densities of the CC mode.

C. Characterisation of MAO Coating

The surface morphology of the MAO coating formed on the aluminium wire at each current density was observed through an M330-HK830 optical microscope (Osmicro Optical Instruments, China). The phase structure and the elemental composition of the MAO coating were identified by using X-ray diffractometry (i.e., XRD, D8 Advance, Bruker, Germany) with a measurement angle range from 10º to 90º (fast scan) and X-ray photoelectron spectroscopy (i.e., XPS, Thermo Fisher, ESCALAB 250 X) respectively [31]. The electrical resistance R_e (Ω) was measured by a VC4090A LCR Digital Bridge Tester (Victory Instruments, China) at temperature of 20 ºC. Given the measurement base length L_w of 0.5 m and the cross-sectional area S (m^2) of the wire, the wire resistivity ρ (Ω·m) can be calculated by (1).

$$\rho = (R_e \cdot S)/L_w \tag{1}$$

D. Mechanical Performance Test

The tensile properties of wire samples were examined using a DR-502A tensile tester (Dongil Instrument Co., Ltd., China). The initial pitch length of sample, tensile speed and temperature were 200 mm, 80 mm/min and 25±1 ºC respectively. In high-temperature tensile tests with gradient heating of 70 ºC, 150 ºC, 200 ºC, 250 ºC and 300 ºC and an applied tension of 25 N, the tensile elongation rates of original aluminium and MAO-treated wire samples were measured.

E. Tribological Test

A steel wool friction resistance tester model 339-GSR II was used to examine the wear performance of the MAO-treated aluminium and the aluminium substrate itself under different lubrication conditions [32]. Considering that the 1.5 mm wire samples would make it difficult to reproduce tribological tests and investigate tribological mechanisms, the aluminium disks which had the same material and type as the aluminium wires but with a diameter of 30 mm and a thickness of 7 mm were used here and treated by the MAO method in the same process as the treatment on the aluminium wires. Then sliding wear tests were performed based on the treated/untreated aluminium disks and 304 stainless steel balls (density 7.93 g/cm^3, diameter 9.525 mm) by the ball-disk contact method at room temperature. The friction coefficients under different lubrication conditions (i.e., dry friction and water lubrication) were determined in the sliding wear process with fixed load and sliding speed equalling 5 N and 1 cm/s respectively. The sliding time duration and displacement amplitude were set to 30 mins and 10 mm respectively. After the sliding wear experiment, the disk and the steel ball were ultrasonically cleaned in anhydrous ethanol and dried with a hair dryer to remove the debris generated by the friction. Then their wear profiles were observed by an optical microscope (A0-V128S, Shenzhen, China), based on which the width of wear tracks on the disk surface and the diameter D_w (mm) of the wear plane left on the steel ball were estimated. Approximating the wear loss of the steel ball by a spherical cap cut off by the plane with the wear diameter D_w, the volume loss V_w (mm^3) of the wear trajectory was estimated by (2).

$$V_w = \pi \cdot h \cdot \frac{3 \cdot \left(\frac{D_w}{2}\right)^2 + h^2}{6} \tag{2}$$

where h denotes the height of the spherical cap equalling $(r - \sqrt{r^2 - (D_w/2)^2})$ given the steel ball radius r (mm). Based on the sliding distance L_s (m) and the testing load F (N), a wear rate W (mm^3·(N·m)$^{-1}$) is estimated by (3) to quantify the wear behaviour [33]. For each disk sample, three friction tests were performed on different sections of the sample, with the average and standard deviation (SD) of the test results being calculated.

$$W = V_w/(F \cdot L_s) \tag{3}$$

F. Neutral Salt Spray Test (NSST)

The NSST was carried out on both original and MAO-treated aluminium samples using a salt spray testing machine produced by Ningbo Oulinte Electromechanical Manufacturing Co., Ltd. The salt mist tester conforms to National Standard GB/T 10587-2006. The samples cleaned by acetone and deionised water were placed on the test rack without any interference between themselves. In addition, a placement angle of 20±5 º relative to the vertical was achieved to optimise the contact area of the sample with the salt spray. The NSST lasted 480 hours during which the NaCl concentration, temperature and pH were kept at 5wt%, 35±2 ºC and 6.8-7.2 respectively.

III. Results and Discussion

A. Characteristics of MAO Coating

1) Microstructure of MAO coating

The surface appearance of the original aluminium (Al) and the MAO-coated aluminium (Al-MAO) samples treated at different current densities is shown in Fig. 3. The Al wire shows a smoother metallic texture with more micro-cracks and surface defects (see Fig. 3(a)), which may account for poor mechanical properties. The Al-MAO surface exhibits a typical volcano-like multi-porous structure without obvious micro-cracks, as shown in Fig. 3(b)-3(g). However, larger pores are found on the Al-MAO surface processed at a higher current density. Fig. 3(h) shows the increase of the pore size with the current density. The Al-MAO sample formed at 0.4 A/dm^2 has a relatively flat surface with a few micro-pores only (see Fig. 3(b)) which have an average diameter of 1.9 μm with a SD of 0.2 μm. The pores on the coating surface treated at 1.6 A/dm^2 show a non-uniform distribution (see Fig. 3(e)) with an average diameter of around 3.1 μm and a SD of 0.1 μm. When treated at 2.4 A/dm^2, irregular pits appear on the rough coating surface with a significant increase in the pore diameter to an average of

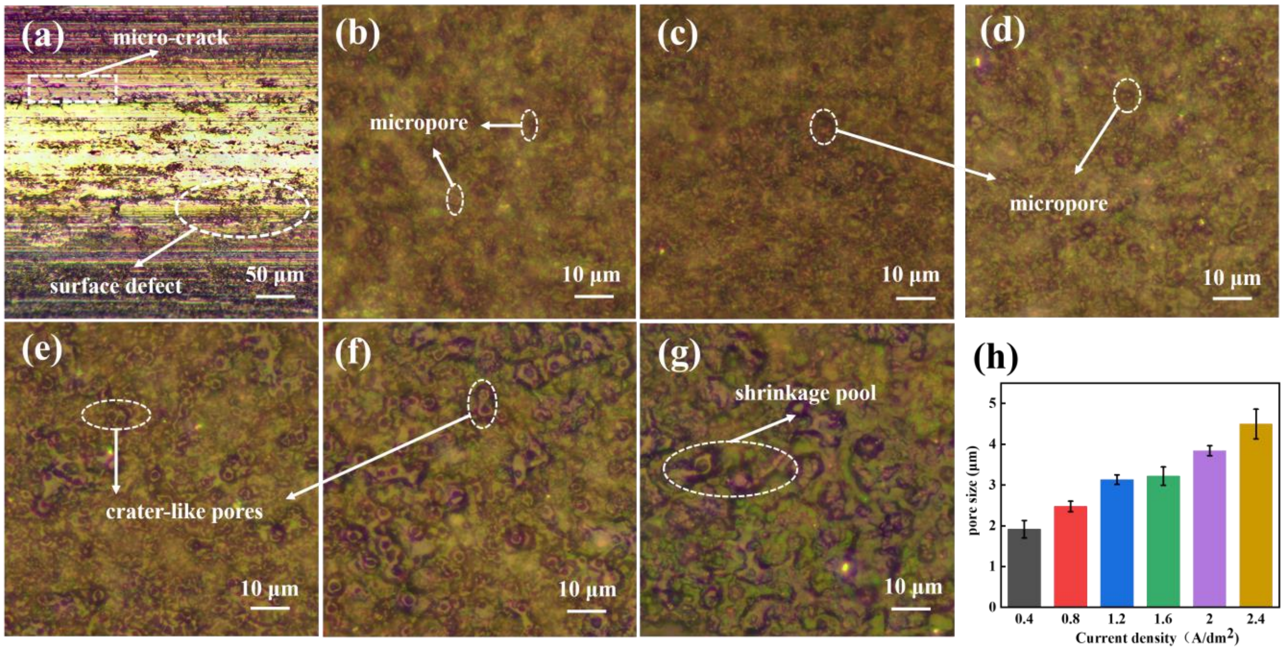

Fig. 3. (a) The surface morphology of the Al wire; (b)-(g) surface microstructure of Al-MAO samples prepared at current density of (b) 0.4 A/dm^2, (c) 0.8 A/dm^2, (d) 1.2 A/dm^2, (e) 1.6 A/dm^2, (f) 2 A/dm^2 and (g) 2.4 A/dm^2; and (h) pore sizes (μm) of MAO coatings prepared at different current densities (A/dm^2).

4.5 μm with a SD of 0.4 μm (see Fig. 3(g)). These micro-pores were created in the MAO process when the intense spark discharge created instantaneous high temperature that caused the oxide film to melt in the discharge channel. Then the molten film turned into gases which would rapidly cool and solidify under the sudden cooling effect of the electrolyte, leaving pores on the coating surface [13], [34]. Given a limited cooling rate, the use of higher current generated more heat and created larger pores, resulting in a rougher coating surface.

2) XRD and XPS analysis

Fig. 4(a) shows the XRD spectra of the Al wire and the Al-MAO wire treated at 1.2 A/dm^2. An intense γ-Al_2O_3 diffraction peak of the Al-MAO locates at 2θ = 64°, with other diffraction peaks complying with those of the Al [35], [36]. The aluminium peaks of MAO coatings may be caused by the penetration of X-rays into the substrate, while other phases may not be detected given their small content. Although a sub-stable γ-Al_2O_3 phase could be converted into a stable α-Al_2O_3 phase at high temperature, this transformation was inhibited by the constant cooling cycle of the electrolyte and the low temperature of the aluminium wire close to the liquid surface.

The chemical state of the coating elements is reflected by the XPS spectra, as shown in Fig. 4(b) where Na, N and Si elements in the electrolyte composition can be observed. Figs. 4(c)-4(f) show the high-resolution profiles of C, Si, Na, and Al elements respectively. The characteristic binding peaks of C 1s at 286.5 eV, 284.6 eV and 282.7 eV are attributed to C-O, C-H and C-O functional groups respectively. The Si 2p signal shows a peak at about 101.2 eV that is contributed by SiO_3^{2-} of the electrolyte composition Na_2SiO_3 [37], while the Na 1s signal exhibits a characteristic peak at an approximate binding energy of 1071.4 eV which is contributed by Na^+ of the electrolyte. Since a large number of ionic elements of the electrolyte were deposited on the sample surface under the high-voltage electric field, more bonds were formed with these elements while the number of bonds formed with aluminium was reduced. Therefore, the peak of Al 2p representing Al_2O_3 is less obvious in comparison and detected at a binding energy of 72.4 eV, which means that the Al element in the coating mainly exists in the form of Al_2O_3 and further explains that the main substance of the oxide layer is alumina [38], [39].

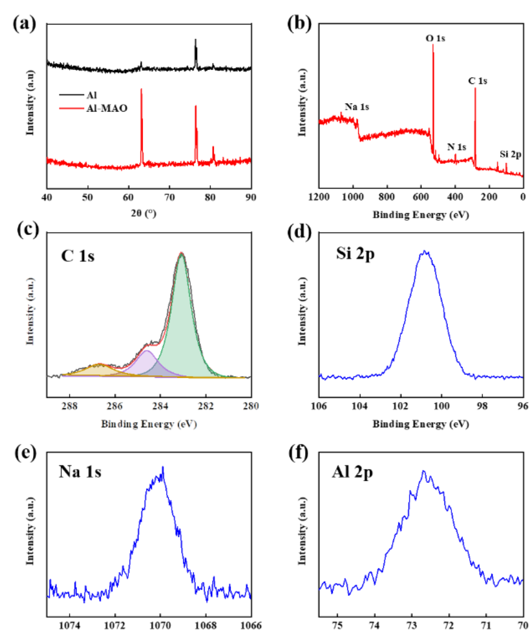

Fig 4. (a) The XRD patterns of the Al and Al-MAO wires treated at 1.2 A/dm^2; XPS spectra of the Al-MAO at (b) full-range scan, (c) C 1s core level, (d) Si 2p core level, (e) Na 1s core level, and (f) Al 2p core level.

3) Mechanical performance at room temperature

The normal operation of OHL conductors will be determined by their mechanical performance. Fig. 5 shows the stress-strain curves of the Al and Al-MAO wires treated at different current densities and compares their tensile strength and elongation at break that are measured at room temperature. Although the MAO treatment does not greatly alter the overall trend of non-linear stress-strain curves of wires, it apparently increases the tensile strength from an average of 162.1 Mpa with a SD of 5.2 Mpa to an average of around 195.6 Mpa with a SD of 3 Mpa (i.e., an increase of 20.7%) given a current density of 1.2 A/dm^2. This is mainly because the inhomogeneous grains within the microstructure of the original Al wire were refined with the rapid heating of the spark discharge and the fast cooling of the electrolyte, resulting in a higher undercooling degree and increasing the wire surface strength. In addition, during the MAO treatment, the thermal expansion of the alumina, together with the crystal lattice mismatch, induced residual stresses between the coating and the substrate surface, which could also improve the mechanical properties of the aluminium substrate. However, the substrate and the ceramic layer underwent plastic transformation and brittle fracture respectively under the applied tension, reducing the plasticity of the Al-MAO wires. This may explain the degradation in the elongation at break after the MAO treatment, as shown in Fig. 5(b). Fortunately, the decline of the elongation at break is small on average, e.g., from an average of 2.43% with a SD of 0.21% for the untreated wire to an average of 2.37% with a SD of 0.12% for the wire treated by the 1.2 A/dm^2 current. Therefore, the MAO process can improve the overall mechanical properties of aluminium wires. Among a variety of current density levels applied in the MAO process, the Al-MAO samples treated by the 1.2 A/dm^2 current gave the best mechanical properties and are selected to present the results of other tests in the following sections for brevity.

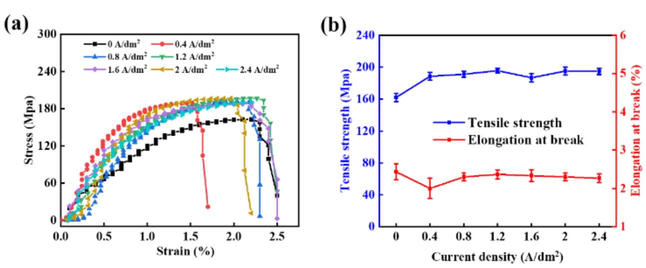

Fig. 5. (a) The stress-strain curves, (b) tensile strength (Mpa) and elongation at break (%) of Al and Al-MAO wires treated at different current densities.

4) Mechanical performance at high temperature

Fig. 6 shows the tensile elongation rates of the Al wire and the 1.2 A/dm^2-based Al-MAO wire measured at different high temperature. Their elongation rates are shown to increase with temperature not only due to the physical change associated with the thermal expansion but also to the binding force changing inside the material under the state of heating. In addition, due to an increased surface hardness mitigating the wire stretching, the MAO treatment is shown to reduce the wire elongation from an average of 1.5% with a SD of 0.03% to an average of 1.15% with a SD of 0.03% at 250 °C and from an average of 2% with a SD of 0.02% to an average of 1.25% with a SD of 0.02% at 300°C. This illustrates that the MAO treatment can mitigate the elongation of aluminium wires at excessive high temperature.

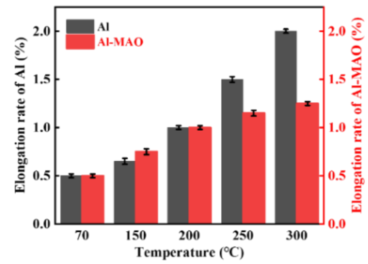

Fig. 6. Elongation rates of Al or 1.2A/dm^2-based Al-MAO at high temperature.

B. Wear and Tribological Properties

1) Wear and tribological properties of wire samples

Fig. 7 shows the sliding wear morphology of the Al substrate and the 1.2 A/dm^2-based Al-MAO under different tribological conditions respectively. The Al sample surface was severely worn under dry friction, showing a large number of long wear grooves along the sliding direction and some fine particles with significant wear and oxidation (see Fig. 7(a)). The wear degree was reduced under water-lubricated condition, with shallower grooves and the overall width of wear reducing from 1658 μm to 743 μm, as shown in Fig. 7(b). This is because a non-uniform contact between the Al sample and the friction sub was formed at the beginning of the mutual friction process, followed by the wearing of some micro-convex bodies under certain load and sliding speed. In dry friction condition, the worn micro-convex bodies created abrasive debris along the wear track, leading to the micro-cutting phenomenon during the sliding friction which accelerated the wear of the aluminium substrate. Under water lubrication, however, the debris were encased in the lubricating medium due to the flowing aqueous solution, reducing their damage to the aluminium substrate.

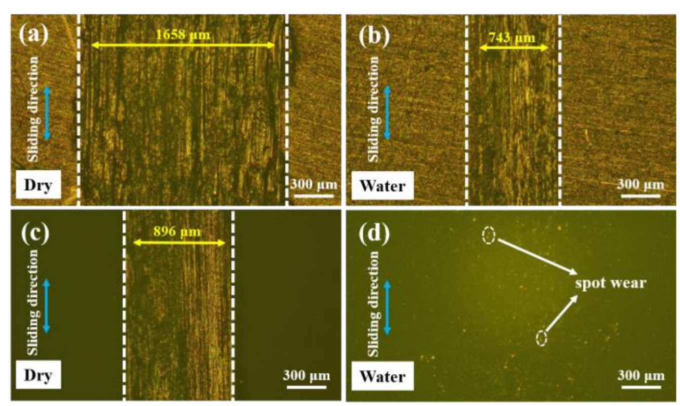

Fig. 7. The sliding wear morphology of Al substrate under (a) dry friction or (b) water lubrication and of 1.2 A/dm^2-based Al-MAO under (c) dry friction or (d) water lubrication.

Figs. 7(c) and 7(d) show that the MAO coating had a reduced wear width and an improved wear resistance due to its higher hardness, especially under the water-lubricated condition where it had an almost unworn surface with a few visible spot scratches only. In addition, the interface bonding of the MAO coating was created in a metallurgical form based on chemical combination and diffusion, which prevented the separation of the film layers and thus effectively reduced the wear damage. Therefore, the MAO treatment can improve the wear resistance of substrates, especially under certain lubrication.

Fig. 8 shows the coefficient of friction (COF) variations of the Al and the 1.2 A/dm^2-based Al-MAO against steel balls in the 30-min sliding wear experiment under the two tribological environments. In the cases of dry friction, the COF of the Al sample dropped from about 1.2 to 0.62 and stabilised after a longer break-in period of 1200 s (see Fig. 8(a)). This may be because the peeling of the softer Al surface was accelerated due to adhesive wear in dry friction. For the Al-MAO samples, the porous part of the ceramic layer was compressed by steel balls and destroyed under high shear stress during the initial sliding process where the COF gradually decreased from 1.1. Then the break-in phase gradually came to an end with the COF stabilising at around 0.75 since 150 s, as shown in Fig. 8(a). However, the COF of the Al-MAO suddenly increased at around 1200 s and then fell to about 0.62 close to that of the Al sample, which may be due to the destruction of the MAO coating leading to a direct contact between the Al substrate and the steel ball. On average, the MAO treatment reduced the COF from 0.81 (with a SD of 0.01) to 0.74 (with a SD of 0.015) under dry friction (see Fig. 8(c)).

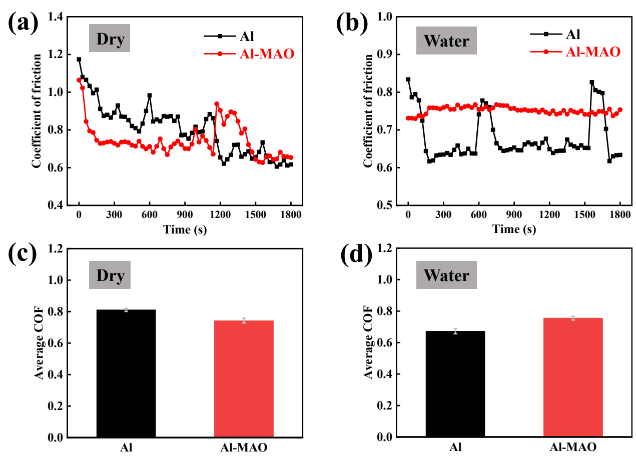

Fig. 8. Coefficients of friction (COF) of Al and 1.2 A/dm^2-based Al-MAO in the sliding process under (a) dry friction and (b) water lubrication and their respective average COF under (c) dry friction and (d) water lubrication.

Under the water-lubricated condition, as shown in Fig. 8(b), the COF of the Al sample rapidly declined within 150 s and then stabilised with some surges. This may be because the debris encased in the lubricating medium acted as rolling balls which reduced the friction of the Al sample. Since the hard and porous surface of the Al-MAO sample was not only less prone to create debris (see Fig. 7(d)) but also had a relatively higher roughness, the COF of the Al-MAO sample was more stable in the sliding process (see Fig. 8(b)) and had an average of 0.76 (with a SD of 0.012) which was greater than the Al-based average COF of 0.67 (with a SD of 0.016), as shown in Fig. 8(d). This also indicates that the Al-MAO samples had an improvement in the wear resistance.

2) Wear properties of steel balls

Figs. 9(a) and 9(c) show the surfaces of the steel balls under dry friction against Al and Al-MAO samples respectively, which were both severely worn with obvious grooves and pits. However, the steel ball sliding against the Al-MAO sample had a smaller wear diameter and a reduced wear rate than the steel ball against the Al sample under dry environment. As shown in Fig. 9(e), the steel balls sliding against the Al or Al-MAO sample were estimated to have an average wear rate of 9.77 (with a SD of 0.5) $\times 10^{-4}$ mm$^3\cdot$(N$\cdot$m)$^{-1}$ or 5.9 (with a SD of 0.75) $\times 10^{-4}$ mm$^3\cdot$(N$\cdot$m)$^{-1}$ respectively. This is because the steel ball with high hardness and high roughness embedded in the softer Al substrate and accelerated the sample surface flaking due to the adhesive wear. With the wear track becoming wider and deeper, the contact area between the steel ball and the Al substrate increased, causing a larger wear rate of the steel ball [40]. In the case of the Al-MAO sample, the presence of the alumina in the hard ceramic layer improved the bearing capacity of the substrate, so that the steel ball was difficult to press into the inner Al substrate under low load, which reduced the wear rate of the steel ball.

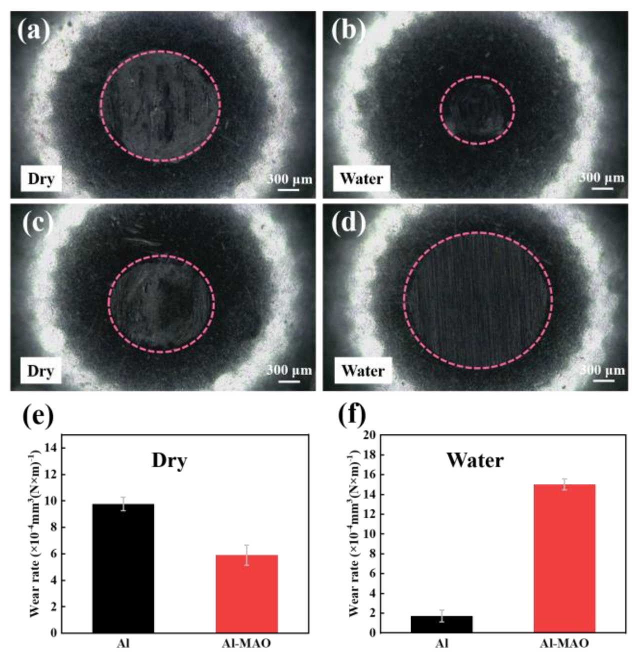

Fig. 9. The wear morphology of steel balls sliding against the Al sample under (a) dry friction and (b) water lubrication and of steel balls against the Al-MAO sample under (c) dry friction and (d) water lubrication; and their corresponding wear rates ($\times 10^{-4}$ mm$^3\cdot$(N$\cdot$m)$^{-1}$) under (e) dry friction and (f) water lubrication.

Under the water-lubricated condition, the contact surface of the steel ball against the Al-MAO sample shows clear scratch marks with an increased wear diameter of about 1976 μm (see Fig. 9(d)), while the steel ball surface against the Al sample has a small wear diameter of around 1141 μm (see Fig. 9(b)). The resulting average wear rate of the steel balls sliding against the Al or Al-MAO sample was estimated to be around 1.7 (with a SD of 0.6) $\times 10^{-4}$ mm$^3\cdot$(N$\cdot$m)$^{-1}$ or 15 (with a SD of 0.55) $\times 10^{-4}$ mm$^3\cdot$(N$\cdot$m)$^{-1}$ respectively, as shown in Fig. 9(f). This might be because the sliding process ground wear debris into powders which were then filled into the pores of the MAO coating under the action of water lubrication, increasing the real contact area of the steel ball with the Al-MAO surface and thus creating wide scratches along the sliding direction.

C. Impact of Corrosion on Al and Al-MAO

1) Microstructure after NSST

To examine the effect of the MAO treatment on the corrosion resistance, the surface appearance of Al and Al-MAO samples prior to and after the NSST is compared in Fig. 10 respectively. The NSST is shown to form red corrosion marks and corrosion pits on the Al sample surface (see Figs. 10(a) and 10(b)), but have insignificant influences on the surface of the Al-MAO sample prepared at a current density of 1.2 A/dm^2 (see Figs. 10(c) and 10(d)) or 2.4 A/dm^2 (see Figs. 10(e) and 10(f)). This is because the molten Al_2O_3 formed in the later stage of the MAO process had no time to be ejected from the discharge channel and would solidify under the cooling effect of the electrolyte, blocking the perforation and making the surface pores impenetrable. When the corrosive mediums entered the coating, their forward path was obstructed by the overlapping microporous distribution within the loose layer, which avoided their contact with inner aluminium substrate and thus improved the corrosion resistance of the treated samples [41]. Therefore, the MAO treatment can be an effective way to keep aluminium conductors from corrosion.

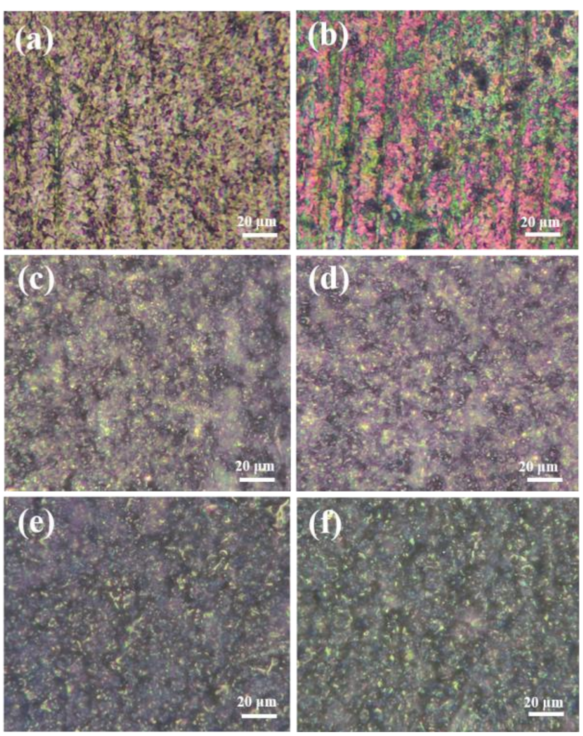

Fig. 10. The surface morphology of (a) pre- and (b) post-NSST Al samples, (c) pre- and (d) post-NSST 1.2 A/dm^2-based Al-MAO samples, and (e) pre- and (f) post-NSST 2.4 A/dm^2-based Al-MAO samples.

2) Electrical resistivity after NSST

Electrical conductivity or resistivity is an important property of conductor materials determining the transmission efficiency of OHLs. The conductivity is sensitive to the microstructure of metallic material and affected by the electron scattering due to disturbances in the crystal structure such as thermal vibrations, impurities, lattice defects, etc. As was noted in Section III.A, the inhomogeneous grains of original Al wires could be refined during the MAO treatment. Even though the grain refinement within the microstructure improved the mechanical properties, it introduced insignificant changes to the wire conductivity, as shown in Fig. 11(a). For example, the original Al wires and the Al-MAO wires treated by the 1.2 A/dm^2 current had an average resistivity of 2.93 (with a SD of 0.03) $\times 10^{-8}\ \Omega\cdot$m and 2.89 (with a SD of 0.04) $\times 10^{-8}\ \Omega\cdot$m respectively which were very similar prior to the NSST. The Al-MAO wire prepared at a greater current density is generally shown to have a slightly higher resistivity, due to its thicker insulating ceramic oxide film that reduced the effective cross-sectional area for the electron flow. The maximum resistivity growth after the MAO treatment is evaluated to be around 2.4% only when a current density of 1.6 A/dm^2 was applied to produce the Al-MAO wires which had an average resistivity of 3.0 (with a SD of 0.03) $\times 10^{-8}\ \Omega\cdot$m. This means that the MAO treatment has an insignificant effect on the resistivity of aluminium wires.

Fig. 11(b) compares the pre- and post-NSST resistivity of the Al and the 1.2 A/dm^2-based Al-MAO samples respectively. The average resistivity of the Al samples decreased to 2.59 (with a SD of 0.08) $\times 10^{-8}\ \Omega\cdot$m after the NSST due to the retention of chloride ions on the metal surface. In contrast, the average resistivity of the Al-MAO samples was slightly changed to 2.85 (with a SD of 0.05) $\times 10^{-8}\ \Omega\cdot$m after the NSST, meaning that the Al-MAO wire was basically corrosion-free in terms of the conductivity with little chloride ions left in the loose layer outside the MAO coating.

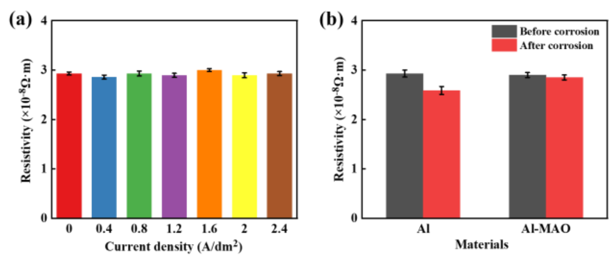

Fig. 11. (a) The Pre-NSST resistivity ($\times 10^{-8}\ \Omega\cdot$m) of Al and Al-MAO samples treated at different current densities and (b) the pre- and post-NSST resistivity ($\times 10^{-8}\ \Omega\cdot$m) of Al and 1.2 A/dm^2-based Al-MAO samples.

3) Wear and tribological properties after NSST

To explore the joint effects of corrosion and wear, the sliding wear tests were carried out on the post-NSST Al and Al-MAO samples under dry friction and water lubrication respectively. The surface morphology of the post-NSST Al and 1.2 A/dm^2-based Al-MAO samples after the sliding wear test is shown in Fig. 12. Given the same friction load, the post-NSST Al sample shows an increased wear width compared to the pre-NSST Al sample, i.e., from 1658 μm (see Fig. 7(a)) to 2537 μm (see Fig. 12(a)) under dry friction or from 743 μm (see Fig. 7(b)) to 1548 μm (see Fig. 12(b)) under the water-lubricated condition. This demonstrates that the salt spray corrosion significantly reduced the wear resistance of the Al sample surface. Under dry friction, the post-NSST Al-MAO also suffered an increased wear width from 896 μm (see Fig. 7(c)) to 1228 μm (see Fig. 12(c)). This may be because the corrosive liquid penetrated into the loose layer of the coating surface and caused damage to the structure of micro-pores in the NSST, which reduced the wear resistance of the coating and thus led to a larger wear width. However, the wear width of the post-NSST Al-MAO is still only around half of that of the post-NSST Al sample under dry friction. Fig. 12(d) shows that the post-NSST Al-MAO sample has sporadic wear traces with almost no wear on its surface under the water-lubricated condition. Therefore, the MAO coating can improve the resistance of the aluminium substrate to the joint effect of corrosion and wear, especially under certain lubrication.

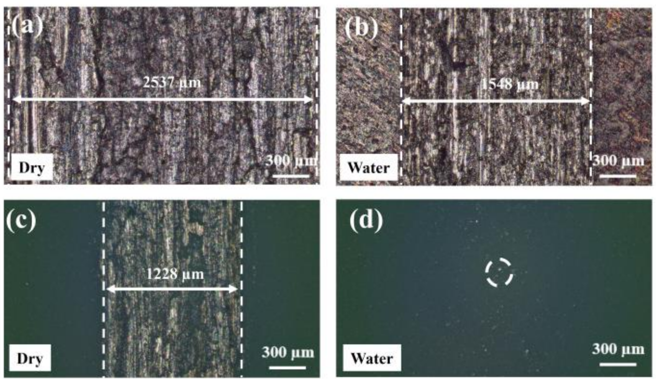

Fig. 12. The wear morphology of post-NSST Al samples under (a) dry friction and (b) water lubrication and of post-NSST 1.2 A/dm^2-based Al-MAO samples under (c) dry friction and (d) water lubrication.

The COF variations of post-NSST Al and 1.2 A/dm^2-based Al-MAO samples during the sliding friction process under dry friction and water lubrication are shown in Figs. 13(a) and 13(b) respectively. The COFs of the post-NSST Al samples fluctuated greatly under both tribological conditions and had a significant trough occurring at around 700 s under dry friction, meaning that the Al surface was prone to be peeled off after the corrosion and was severely destroyed by the steel ball. For the Al-MAO samples, the post-NSST COF continuously increased at the start of dry friction (see Fig. 13(a)), which is different from the initial drop of the pre-NSST COF (see Fig. 8(a)). This may be because the corrosive liquid penetrating into the loose layer of the MAO coating reduced the hardness of the coating surface, so that the steel ball gradually contacted the inside of the coating, resulting in an increasing COF during the initial dry friction. Under water lubrication, the post-NSST Al-MAO had relatively stable COFs (see Fig. 13(b)) with an average of 0.73 and a SD of 0.05 (see Fig. 13(d)) which is similar to the pre-NSST Al-MAO sample. This illustrates that the salt spray corrosion had little effect on the COF of the MAO coating given certain lubrication.

D. Relevant Mechanisms

Based on the experimental results discussed in the sections above, the main mechanisms related to the improvement of Al wire resistance to wear and corrosion by the MAO treatment are summarised in Fig. 14. The high hardness and roughness of the steel ball make itself easily embed in the soft Al substrate, causing fatigue cracks and fracture flakes in the substrate during

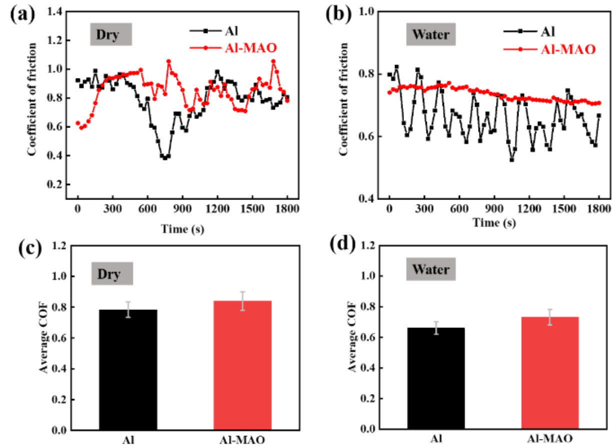

Fig. 13. Coefficients of friction (COF) of post-NSST Al and 1.2 A/dm^2-based Al-MAO in the sliding process under (a) dry friction and (b) water lubrication and their respective average COF under (c) dry friction and (d) water lubrication

the frictional wear. When using the MAO technology to process an Al wire, the high-temperature molten oxide is formed on the wire surface and ejected from the discharge channel, and finally cooled and solidified under the action of the electrolyte. The outer layer of the coating directly contacting with the electrolyte experiences a higher cooling rate, forming a loose and porous γ-Al_2O_3 ceramic structure. The improved resistance of the Al-MAO wire to both wear and corrosion can be attributed to the shielding of the MAO coating with special phase structure and morphology. The MAO coating mainly consisting of Al_2O_3 has a high hardness degree and thus effectively increases the wear resistance of conductors. In addition, during the sliding friction process, the brittle ceramic coating will be partially shed into fine abrasive particles which then fill in the micro-pores of the coating surface and thus change the adhesive wear mechanism of the original aluminium wire, providing a more effective wear protection under water lubrication. In a corrosive environment, the overlapping micro-porous distribution in the loose layer of the coating can hinder the penetration of the corrosive mediums into to the inner aluminium substrate, effectively improving the corrosion resistance of aluminium conductors.

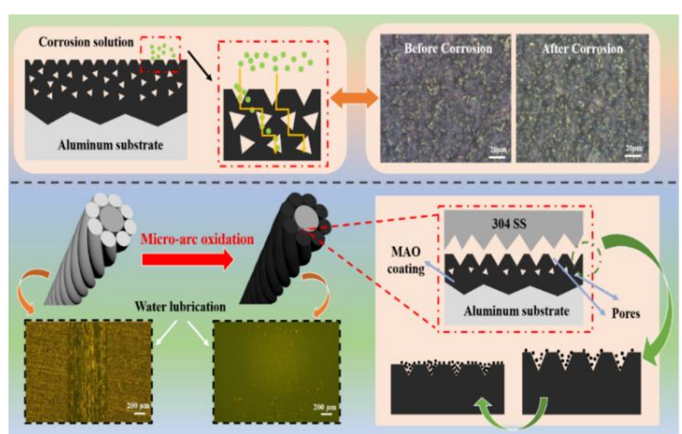

Fig. 14. Diagram of main mechanisms about the MAO treatment on aluminium conductors to improve wear and corrosion resistance.

E. Discussions on Al-MAO Application and Benefits

The aluminium wire sample treated in this study was 500 mm long only. When dealing with the treatment of long aluminium wires, the application of the proposed MAO method could be realised by moving the unpowered end of the wire to immerse the untreated section into the electrolyte and generating MAO coatings along the wire in sequence. An alternative approach could develop a novel MAO equipment set that sprays the electrolyte through a mobile nozzle (which can move in any direction) onto the wire where coatings will be formed. These can help avoid the use of excessively large electrolyte tanks and high currents. In addition, due to the brittleness of the MAO coating, twisting the coated wires into a cable may cause serious cracks which affect the corrosion stability of the cable. In order to avoid the use of high currents producing more brittle coatings that are prone to cracking, the MAO treatment method proposed here is regulated by a CV mode followed by a CC mode, as was described in Section II.B. This can achieve the voltage level that initiates the MAO process while ensuring a low current density. Fig. 15 shows the simulation of twisting a coated wire into a cable and the resulting micromorphology of the coating surface which still exhibited a porous structure without obvious cracks. Therefore, the use of small current density in the MAO process can help reduce the brittleness of the MAO coating and mitigate the occurrence of severe cracks when twisting wires into a cable.

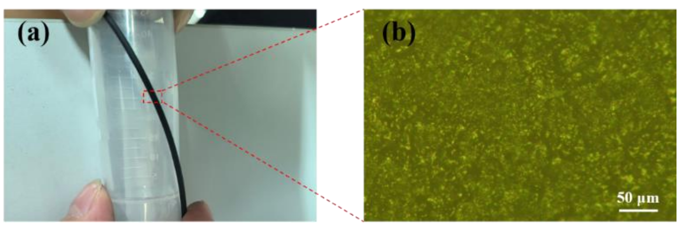

Fig. 15. (a) The simulation of twisting a coated wire into a cable and (b) the resulting micromorphology of the coating surface.

As was discussed above, the improved resistance to wear and corrosion by the MAO treatment can increase the service life of aluminium conductors and alleviate maintenance needs, which will help defer the requirement of conductor replacement and reduce maintenance costs in practice. To reflect the economic benefits of the MAO treatment, the overall annual costs C_{ann}^{tot} of a particular 10 kV, 4.9 km OHL comprising LGJ-240/40 ACSR conductors [42] are estimated by:

$$C_{ann}^{tot} = O_i + O_m + \frac{d}{1-(1+d)^{-N}} \cdot \left(C_{wire}^{eqpt} + C_{wire}^{accs} + C_{wire}^{d\&i} + C_{wire}^{oth} + C_{MAO}^{eqpt} + C_{MAO}^{elyt} + C_{MAO}^{kWh}\right) \quad (4)$$

where d and N denote an interest rate of 5% and the service life (years) of the line respectively. The term $d/(1-(1+d)^{-N})$ is a capital recovery factor applied to the one-off investments into wires C_{wire}^{eqpt}, wire accessories C_{wire}^{accs}, design and installation $C_{wire}^{d\&i}$ and other wire-related items C_{wire}^{oth}, as well as the MAO equipment set cost C_{MAO}^{eqpt} and consumptions of electrolyte C_{MAO}^{elyt} and electricity C_{MAO}^{kWh} for MAO treatment. Terms O_i and O_m are annual costs of inspection and maintenance respectively which depend on the inspection and maintenance cycles per year. The techno-economics of the 10 kV OHL and the MAO treatment are tabulated in Table I. Compared with the untreated line, the MAO-coated line is presumed to operate for 10 more years [43] and require less frequent maintenance activities.

TABLE I
TECHNO-ECONOMICS OF ORIGINAL AND MAO-TREATED CONDUCTORS.

Item	Original	MAO-Treated
Line Length (m)	4,908	4,908
No. of Al Strands	26	26
Al Strand Diameter (mm)	3.42	3.42
Service Life (year)	30	40
Wire Cost (CNY)	288,000	288,000
Wire Accessory Cost (CNY)	77,200	77,200
Wire Design & Installation Cost (CNY)	865,500	865,500
Other Wire-related Cost (CNY)	34,000	34,000
10 kW MAO Equipment Set Cost (CNY)	N/A	60,000
MAO Electrolyte Cost (CNY/m^2 of SA)†	N/A	9.88
MAO Electricity Cost (CNY/m^2 of SA)*	N/A	3.18
Inspection Cost (CNY/time)	18,800	18,800
Inspection Cycle (times/annum)	1	1
Maintenance Cost (CNY/time)	4,960	4,960
Maintenance Cycle (times/annum)	12	4 – 12

† based on that the MAO treatment on aluminium wires with an overall surface area (SA) of 100 m^2 consumes around 675 L of electrolyte, worth 988.2 CNY.
* based on that the MAO treatment on an aluminium wire of 1.5 mm diameter, 500 mm length and 0.0024 m^2 SA consumes around 0.015 kWh of electricity, worth 0.0075 CNY.

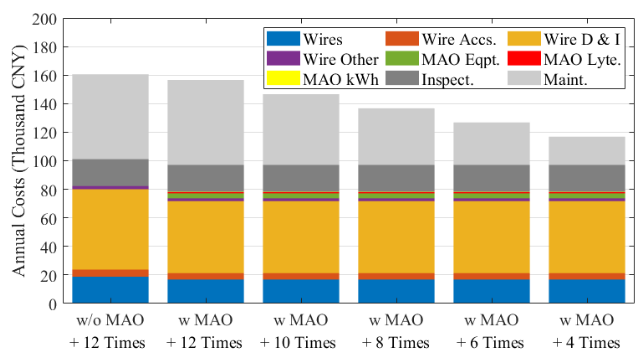

Fig. 16. Overall annual costs (thousand CNY) of untreated and MAO-treated OHLs given different maintenance cycles per annum.

Fig. 16 shows the overall annual costs estimated for untreated OHLs and MAO-coated OHLs where the maintenance would be carried out 4 to 12 times per annum. Although the MAO treatment causes additional equipment set costs of 60 thousand CNY, electrolyte consumptions of 13.5 thousand CNY and electricity usage of 4.4 thousand CNY, the overall capital expenditures (CAPEX) associated with the MAO treatment contribute 5.8% only to the total CAPEX of the treated OHL in this case. Furthermore, the extended service life of the treated line leads to a smaller capital recovery factor and a reduction of around 4 thousand CNY in the total CAPEX annuitised across the service life. In addition, depending on the maintenance schedule adopted by the electric network owner, the decrease of maintenance activities could make the main contribution to the total annual cost saving of the MAO-treated OHL. Fig. 16 shows that the overall annual cost would drop by about 8.7% or 27.2% (i.e., 13.9 or 43.7 thousand CNY) given the maintenance being performed ten or four times per annum respectively. It is noted that the MAO equipment set costs dominating the overall MAO-related CAPEX would decline with the mass production of MAO-coated lines, ensuring the cost-effectiveness of the MAO technology.

IV. Conclusion

This paper has described the preparation of ceramic coatings on high-voltage (HV) aluminium (Al) conductors by the micro-arc oxidation (MAO) technology. The surface morphology, mechanical properties and electrical resistivity of the MAO-coated wires prepared at different current densities in the MAO process have been investigated. In addition, the frictional wear properties and the corrosion resistance of MAO-coated samples have been examined and compared with those of the original Al samples. The key findings of this research are:

1) The current density adopted in the MAO process affects the microstructure of the MAO coating. When a typical volcano-like porous structure appears on the coating surface, increasing the current density would gradually enlarge the pore size and fluctuate the number of pores.
2) The MAO-coated wire has an improved tensile strength, which increases by 20.7% relative to the original Al wire given the use of 1.2 A/dm^2 current density. In addition, the MAO treatment largely reduces the wire elongation at excessive high temperature, with an elongation rate of around 1.2% only at 250^{o}C and 300^{o}C.
3) The MAO treatment has little influence on the electrical conductivity of the wire, with a resistivity growth of less than 2.4%. Furthermore, due to the overlapping micro-porous distribution in the loose layer, the MAO coating can prevent corrosive mediums from penetrating into the inner Al substrate and affecting the conductivity.
4) Under the low-speed, low-load sliding friction against stainless steel balls, the MAO treatment reduces the extent and width of the wear on the sample surface, with almost no wear given certain lubrication. In addition, the MAO coating is effective in protecting the Al substrate from the corrosion in the neutral salt spray test (NSST). Although the protective effect of the coating is reduced due to the corrosion, the post-NSST MAO coating still provides certain wear resistance. Therefore, the MAO treatment can effectively inhibit the joint effects of wear and corrosion.
5) The MAO treatment can help increase the service life of HV Al conductors and reduce maintenance needs. Given a service life extension of 10 years and a reduced maintenance cycle from 12 times to 4 times per annum, it is evaluated that around 27.2% of the overall annual cost of a particular 10 kV, 4.9 km overhead line can be saved by the application of the MAO technology.

References

[1] H. Y. Li, J. Y. Duan, and D. D. Wei, "Comparison on corrosion behaviour of arc sprayed and zinc-rich coatings," *Surface and Coatings Technology,* vol. 235, pp. 259-266, 2013.

[2] K. Y. Sik, K. k. tae, and Y. Yoo, "Accelerated Prediction Methodologies to Predict the Outdoor Exposure Lifespan of Galvannealed Steel," *Corrosion Science and Technology,* vol. 18, no. 3, pp. 86-91, 2019 2019.

[3] H. Niu, X. Li, and W. Zhang, "Capacity assessment of existing corroded overhead power line structures subjected to synoptic winds," *Wind and Structures,* vol. 27, no. 5, pp. 325-336, Nov 2018.

[4] V. F. Steier, M. S. T. Pires, and T. Doca, "The influence of diamond-like carbon and anodised aluminium oxide coatings on the surface properties of the SAE 305 aluminium alloy," *Journal of the Brazilian Society of Mechanical Sciences and Engineering,* vol. 40, no. 2, 2018.

[5] X. Ma, L. Gao, J. Zhang, and L.-C. Zhang, "Fretting Wear Behaviors of Aluminum Cable Steel Reinforced (ACSR) Conductors in High-Voltage Transmission Line," *Metals,* vol. 7, no. 9, Sep 2017, Art. no. 373.

[6] C. Du, H. Zhao, Z. Dai, Z. Tian, J. Wang, and Z. Wang, "The preparation and properties of black coating by micro arc oxidation on 2A12 aluminum alloy," *Materials Letters,* vol. 236, pp. 723-726, Feb 1 2019.

[7] P. Wang *et al.*, "Effects of Al2O3 Micro Powder Addition Amount on Characteristics of Micro-arc Oxidation Coating Formed on Magnesium Alloy," *Rare Metal Materials and Engineering,* vol. 46, no. 5, pp. 1260-1264, May 2017.

[8] M. M. Ma, Y. Q. Wen, W. Shang, and J. P. Li, "Preparation and Corrosion Resistance of Micro-arc Oxidation/Self-Assembly Composite Film on 6061 Aluminum Alloy," *International Journal of Electrochemical Science,* vol. 14, no. 12, pp. 11731-11743, Dec 2019.

[9] L. Guo *et al.*, "The effect of relative humidity change on atmospheric pitting corrosion of stainless steel 304L," *Corrosion Science,* vol. 150, pp. 110-120, Apr 15 2019.

[10] Q. Li, J. Lin, C. Li, S. Lu, and X. Chen, "Effect of relative humidity on corrosion behavior of SAC305 and Sn-37Pb solders under polyvinyl chloride fire smoke atmosphere," *Journal of Materials Science-Materials in Electronics,* vol. 31, no. 22, pp. 19920-19930, Nov 2020.

[11] L. Guo *et al.*, "Effect of Mixed Salts on Atmospheric Corrosion of 304 Stainless Steel," *Journal of the Electrochemical Society,* vol. 166, no. 11, pp. C3010-C3014, Jan 9 2019.

[12] M. Jakubowski, "INFLUENCE OF PITTING CORROSION ON FATIGUE AND CORROSION FATIGUE OF SHIP AND OFFSHORE STRUCTURES, PART II: LOAD - PIT - CRACK INTERACTION," *Polish Maritime Research,* vol. 22, no. 3, pp. 57-66, 2015 2015.

[13] Q. Guo *et al.*, "Synthesis, corrosion, and wear resistance of a black microarc oxidation coating on pure titanium," *Surface and Coatings Technology,* vol. 386, 2020.

[14] P. de Kol, G. K. R. Pereira, S. Fraga, N. de Jager, A. B. Venturini, and C. J. Kleverlaan, "The effect of internal roughness and bonding on the fracture resistance and structural reliability of lithium disilicate ceramic," *Dental Materials,* vol. 33, no. 12, pp. 1416-1425, Dec 2017.

[15] Q. Lin *et al.*, "Enhancement of Si3N4@MoS2 core-shell structure on wear/corrosion resistance of epoxy resin/polyacrylate IPN composite coating," *Applied Surface Science,* vol. 568, Dec 1 2021, Art. no. 150938.

[16] J. Xiao, C. Lu, S. Jiang, and Y. Li, "Research and Application of Anticorrosive Coating for Reinforced Concrete of Coastal Buildings," *Journal of Coastal Research,* pp. 417-421, Sum 2020.

[17] F. Cirisano, A. Benedetti, L. Liggieri, F. Ravera, E. Santini, and M. Ferrari, "Amphiphobic coatings for antifouling in marine environment," *Colloids and Surfaces A: Physicochemical and Engineering Aspects,* vol. 505, pp. 158-164, 2016.

[18] S. Fang, J. Zhou, S. Huang, Z. Hu, and W. Li, "Evaluation on the Corrosion and Wear Properties of C-Fibers Doped Aluminum Coatings Obtained Using Arc Spray Technolgoy," *Coatings,* vol. 10, no. 11, Nov 2020, Art. no. 1096.

[19] T. F. A. Santos, G. C. Vasconcelos, W. A. de Souza, M. L. Costa, and E. C. Botelho, "Suitability of carbon fiber-reinforced polymers as power cable cores: Galvanic corrosion and thermal stability evaluation," *Materials & Design (1980-2015),* vol. 65, pp. 780-788, 2015.

[20] M. Zhang, J. Zhou, G. Zhao, J. Xu, and C. Sun, "Study of structural-thermal characteristics of electrified conductors under aeolian vibration," *Wind and Structures,* vol. 33, no. 2, pp. 155-168, Aug 2021.

[21] P. Wang *et al.*, "Effects of Indium Sulfide on the Structure and Corrosion Resistance of the Micro-arc Oxidation Coating on ZL108 Alloy," *Rare Metal Materials and Engineering,* vol. 50, no. 1, pp. 56-62, Jan 2021.

[22] Y. Li, M. Chen, W. Li, Q. Wang, Y. Wang, and C. You, "Preparation, characteristics and corrosion properties of alpha-Al2O3 coatings on 10B21 carbon steel by micro-arc oxidation," *Surface & Coatings Technology,* vol. 358, pp. 637-645, Jan 25 2019.

[23] H. Zhu, X. Li, X. Guan, and Z. Shao, "Effect of Molybdate Conversion Coating of Magnesium Alloy Reinforced by Micro-arc Oxidation," *Metals and Materials International,* vol. 27, no. 10, pp. 3975-3982, Oct 2021.

[24] Y. Gong *et al.*, "Self-healing performance and corrosion resistance of novel CeO2-sealed MAO film on aluminum alloy," *Surface and Coatings Technology,* vol. 417, 2021.

[25] S. Ji *et al.*, "Excellent corrosion resistance of P and Fe modified micro-arc oxidation coating on Al alloy," *Journal of Alloys and Compounds,* vol. 710, pp. 452-459, 2017.

[26] Z. Li and S. Di, "Preparation and properties of micro-arc oxidation self-lubricating composite coatings containing paraffin," *Journal of Alloys and Compounds,* vol. 719, pp. 1-14, 2017.

[27] K. Zhou, F. Xie, X. Wu, and S. Wang, "Research Progress on Tribological Properties of Micro Arc Oxidation Coatings on Aluminum, Magnesium and Titanium Based Materials," *Rare Metal Materials and Engineering,* vol. 48, no. 11, pp. 3753-3763, Nov 2019.

[28] H. Li, Z. Song, and P. Tang, "Preparation and Property of Modified Micro-arc Oxidation Coating Using Al2O3 Particles on Ti6Al4V," *Rare Metal Materials and Engineering,* vol. 49, no. 3, pp. 755-760, Mar 2020.

[29] L. Yao, J. Shi, Z. Liu, S. Zhang, B. Qu, and R. Zhang, "Influence of Calcium Glycerophosphate on Properties of Micro Arc Oxidation Coatings Formed on Magnesium Calcium Alloys," *Rare Metal Materials and Engineering,* vol. 43, pp. 302-305, Sep 2014.

[30] H. Guo, Z. Liu, Y. Wang, and J. Li, "Tribological mechanism of micro-arc oxidation coatings prepared by different electrolyte systems in artificial seawater," *Ceramics International,* vol. 47, no. 6, pp. 7344-7352, 2021.

[31] Z. Feng, F. Hu, L. Lv, L. Gao, and H. Lu, "Preparation of ultra-high mechanical strength wear-resistant carbon fiber textiles with a PVA/PEG coating," *RSC Advances*, vol. 41, no. 11, pp. 25530-25541, 2021.

[32] F. Hu, H. Lu, Z. Ye, S. Zhang, W. Wang, and L. Gao, "Slow-release lubrication of artificial joints using self-healing polyvinyl alcohol/polyethylene glyol/graphene oxide hydrogel," *Journal of the Mechanical Behavior of Biomedical Materials*, vol. 124, p. 104807, 2021.

[33] Z. Ye, H. Lu, E. Jia, J. Chen, and L. Fu, "Organic solvents enhance polyvinyl alcohol/polyethylene glycol self-healing hydrogels for artificial cartilage," *Polymers Advanced Technologies*, vol. 33, no. 10, pp. 3455-3469, 2022.

[34] D. Zhang, Y. Ge, G. Liu, F. Gao, and P. Li, "Investigation of tribological properties of micro-arc oxidation ceramic coating on Mg alloy under dry sliding condition," *Ceramics International,* vol. 44, no. 14, pp. 16164-16172, 2018.

[35] L. Shao, H. Li, B. Jiang, C. Liu, X. Gu, and D. Chen, "A Comparative Study of Corrosion Behavior of Hard Anodized and Micro-Arc Oxidation Coatings on 7050 Aluminum Alloy," *Metals,* vol. 8, no. 3, 2018.

[36] X.-J. Li *et al.*, "Microstructure and wear resistance of micro-arc oxidation ceramic coatings prepared on 2A50 aluminum alloys," *Surface and Coatings Technology,* vol. 394, 2020.

[37] S. Guan, M. Qi, C. Wang, S. Wang, and W. Wang, "Enhanced cytocompatibility of Ti6Al4V alloy through selective removal of Al and V from the hierarchical micro-arc oxidation coating," *Applied Surface Science,* vol. 541, 2021.

[38] Q. Chen, W. Li, K. Ling, and R. Yang, "Effect of Na2WO4 addition on formation mechanism and microstructure of micro-arc oxidation coating on Al-Ti double-layer composite plate," *Materials & Design,* vol. 190, 2020.

[39] S. Wang, L. Zhou, C. Li, Z. Li, H. Li, and L. Yang, "Micrographic Properties of Composite Coatings Prepared on TA2 Substrate by Hot-Dipping in Al–Si Alloy and Using Micro-Arc Oxidation Technologies (MAO)," *Coatings,* vol. 10, no. 4, 2020.

[40] R. Gecu, Y. Yurekturk, E. Tekoglu, F. Muhaffel, and A. Karaaslan, "Improving wear resistance of 304 stainless steel reinforced AA7075 aluminum matrix composite by micro-arc oxidation," *Surface and Coatings Technology,* vol. 368, pp. 15-24, 2019.

[41] K. Zhang and S. Yu, "Preparation of wear and corrosion resistant micro-arc oxidation coating on 7N01 aluminum alloy," *Surface and Coatings Technology*, vol. 388, 2020.

[42] Z. Zhu, S. Lu, B. Gao, T. Yi, and B. Chen, "Life cycle cost analysis of three types of power lines in 10 kV distribution network," *Inventions*, vol. 1, no. 4, 2016.

[43] J.S. Forrest and J. M. Ward, "Service experience of the effect of corrosion on steel-cored-aluminium overhead-line conductors," vol. 101, no. 81, pp. 271-283, 1954.

Zhonglei Shao received the B.Eng. and M.Sc. degrees in electronic and electrical engineering from the Shanghai University of Electric Power, Shanghai, China, and the University of Strathclyde, Glasgow, U.K., respectively.

He is now a Ph.D. candidate with the University of Strathclyde focusing on the techno-economic optimisation of renewable energy systems including energy storage. His research area also includes micro-arc oxidation coating applied on transmission cables.

Zishuo Ye received the B.Sc. degree in process equipment and control engineering from Xi'an Polytechnic University, Xi'an, China, in 2020. He has joined the Group of Mechanical and Biomedical Engineering, College of Mechanical and Electronic Engineering, Xi'an Polytechnic University as a master student since September 2020.

His main research interests include friction and lubrication of polymer materials, and micro-arc oxidation for surface treatment of valve metals and applications.

Hailin Lu received the Ph.D. degree in mechanical engineering from Xi'an Jiaotong University, Xi'an, China in 2019, and was awarded the "National Scholarship Certificate for Doctoral Students" issued by the Ministry of Education of P.R. China during his Ph.D. study.

He has been an Associate Professor, a master supervisor, and the leader of an independent research group (PI) with Xi'an Polytechnic University, Xi'an, China since 2019. He is mainly devoted to the engineering tribology research, including AI-aided design and advanced parts manufacturing, multi-scale modelling of surface texture and associated algorithm and optimsiation for revealing the influence of surface texture on surface tribological properties, as well as the effect of micro-arc oxidation of valve metal surface on tribological properties under mixed lubrication conditions.

Fulin Fan received the B.Eng. and Ph.D. degrees in electronic and electrical engineering from North China Electric Power University, Baoding, China, and the University of Strathclyde, Glasgow, U.K., in 2012 and 2018, respectively.

From 2016 to 2018, he was a Research Assistant with the University of Strathclyde, where he has been a Research Associate since 2018. His research interests include real-time thermal rating of overhead lines, energy storage scheduling and optimisation, and transportation electrification.